POD study of aerated cavitation in a venturi nozzle

P. Tomov, Amélie Danlos, S. Khelladi, Florent Ravelet, C. Sarraf, F. Bakir

POD study of aerated cavitation in a venturi nozzle

P. Tomov[1], A. Danlos[2], S. Khelladi[1], F. Ravelet[1], C. Sarraf[1], F. Bakir[1]

[1]DynFluid Laboratory, Arts et Métiers ParisTech
151, Boulevard de l'Hôpital, 75013 Paris, FRANCE
[2]National Conservatory of Arts and Crafts,
292, Saint-Martin Str., 75003 Paris, FRANCE

E-mail: Petar.TOMOV@ensam.eu

Abstract. The fact of injecting bubbles into a cavitating flow influences typical cavitating behavior. Cavitation and aerated cavitation experiments has been carried out on a symmetrical venturi nozzle with convergent/divergent angles of 18° and 8°, respectively. A snapshot Proper Orthogonal Decomposition (POD) technique is used to identify different modes in terms of discharge flow velocity, pressure and injected quantity of air. The energy spectrum per given mode is also presented. The first four modes are outlined in the present paper for an aerated and non-aerated cavitating flows.

1. Introduction

Aerated cavitating flow contains numerous coexisting flow regimes. By nature, the cavitation has an aggressive behaviour and it is capable of doing severe damage to adjacent structures. Controlling cavitation behaviour can help produce a stable regime as opposed to an unstable one. For this purpose, passive control methods based on surface roughness have been studied [1]. Another recently used technique influencing the cavitation inception is the aeration of the flow [2]. In order to reveal and explore those aerated cavitating regimes, a snapshot Proper Orthogonal Decomposition (POD) analyses have been conducted [3,4]. Different modes have been discovered, as a result. Consequently, it is possible to reproduce the factors required to rebuild the dynamic structures as a time-dependent mixture of modes. The paper is organized in four paragraphs. The experimental set-up is described in §2, followed by the results in §3 and conclusion in §4.

2. Experimental Set-up

2.1. DynFluid Laboratory small water test loop

The experiments are conducted in a closed loop test rig (see figure 1). Two 150 - liter storage tanks supply water to the rig. The centrifugal pump impels the flow from constantly full tank 1 to tank 2. Its maximum flow rate capacity is 8 m^3/h. The cylindrical pipe has an inner diameter equal to $D = 40$ mm. Throughput is monitored by a turbine flow meter, followed by the air injection ring. The transparent symmetrical venturi nozzle is placed in the test section (see figure 1), between the two tanks. The converging/diverging angles are 18° and 8°, respectively. The inlet venturi height is $H_{inlet} = 30$ mm and its throat height is $H_{throat} = 10$ mm,

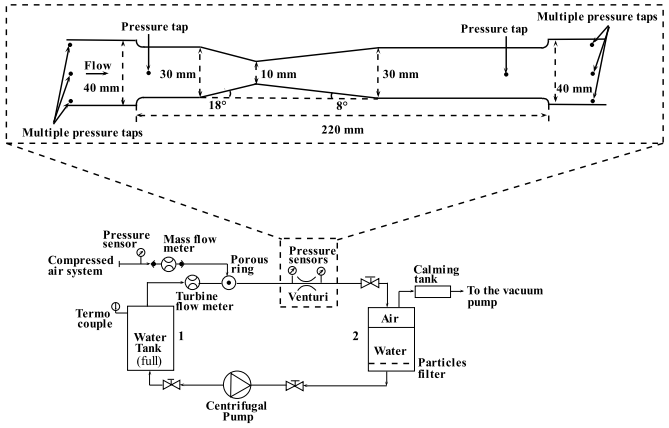

Figure 1. Test rig (not to scale)

which gives an aspect ratio of 3. The total length of the venturi test nozzle is 220 mm. A vacuum pump is connected to tank 2, for the purpose of mitigating the pressure at the free surface. In this way, it is possible to impact the cavitation number, defined as $\sigma = (P_{ref} - P_{vap}) / \left(1/2\rho V_{ref}^2\right)$. All positions X^*, Y^* in the test section are adimensionalized by H_{throat}. The reference pressure P_{ref} is measured at the inlet of the venturi section at $X^* = 6$ from the throat. The discharge velocity V_{ref} is calculated as a function of the flow rate. The vapor pressure in operating conditions is considered 2200 Pa at 19°C.

2.2. Measuring instruments and image capturing technique

Pressure measurements are taken using two absolute pressure sensors, mounted on the inlet and outlet sections at $X^* = 6$ upstream the throat, and $X^* = 10$ downstream the throat. An absolute pressure sensor is mounted on tank 2. The range of working values is from 0 to 2 bar. The uncertainty of the measurements on σ is $\frac{\Delta\sigma}{\sigma} = 0.22$.

Temperature is monitored by a thermocouple mounted on water tank 1. The working range is set to 0°C to 100°C. During all the experimental work, fluid temperature is monitored and maintained to 19°C ± 1°C. In the article, a temperature of 19° will be assumed, giving an uncertainty value of $\frac{\Delta P_{vap}}{P_{vap}} = \pm 0.06$.

Discharge flow rate is monitored by a turbine flow meter, with 10D straight pipe upstream and 5D downstream. The latter is calibrated for a working range of viscosities in the interval 0.6 to 10 cSt. The volume flow rate fluctuation is $\frac{\Delta Q_{liq}}{Q_{liq}} = \pm 0.08$.

Air injection is produced using a compressed air system. Two air filters have been mounted before and after the air mass flow rate meter. The filtration is equal to 5 μm. Volume flow rate fluctuations is $\frac{\Delta Q_{gaz}}{Q_{gaz}} = \pm 0.05$. It has been verified that neither the turbine flow meter nor the non-intrusive injection approach generate any flow perturbations in front of the venturi nozzle. The upstream fluid flow does not content any bubbles as a result of an early cavitation or out-gassing phenomenon.

A CamRecord 600 camera with a 100 mm Zeiss Makroplanar objective lens is mounted on a tripod to insulate it from vibrations that might cause field capturing perturbations. The frequency sample rate is 1 kHz with an exposure time set to 1/40000 s. A total number of 6554 images were taken. The flow was illuminated by a LED backlight.

3. Results and Discussions

Table 1 summarizes the experimental data conditions. Two cases are presented: pure cavitation and aerated cavitation. The variable β, defined as $\beta = Q_{gas}/(Q_{gas} + Q_{liq})$, describes the ratio of injected gas to total volume. The Reynolds number at the venturi throat $Re = V_{ref}.H_{throat}/\nu$ is based on the local flow velocity and the throat height. The Strouhal number Str_L is based on the cavity length on the bottom part of the nozzle in aerated case. All of the images are normalized using a reference image taken at non-cavitating non-aerated flow conditions. The POD analyses in this work follows the one described in [4]. In order to minimize post-processing time, a convergence study is conducted on the minimum number of required images [4,5]. As a

Table 1. Aerated cavitation experimental data table

V_{ref} (m/s)	P_{ref} (bar)	P_{Tank2} (bar)	β	Re	σ	Str_L
11.07	1.10	0.9	0	1.1×10^5	1.78	0.431
11.07	1.04	0.8	0.004	1.1×10^5	1.69	0.352

result, $N = 700$ is taken for the reconstruction of the flow dynamics, as it can be seen in figure 2 (the same result has been found for modes 1 to 3). The information gathered is decomposed into empirical eigenfunctions φ_i. As a result, only a small number of modes are needed to represent correct dynamical evolution of fluid flow. The energy contribution per mode is defined as $E_{mode} = \lambda_i / \sum_{i=1}^{N} \lambda_i$, where λ_i is the eigenvalue after a singular value decomposition for mode i and N is the number of images. The total number of studied modes is equal to 10.

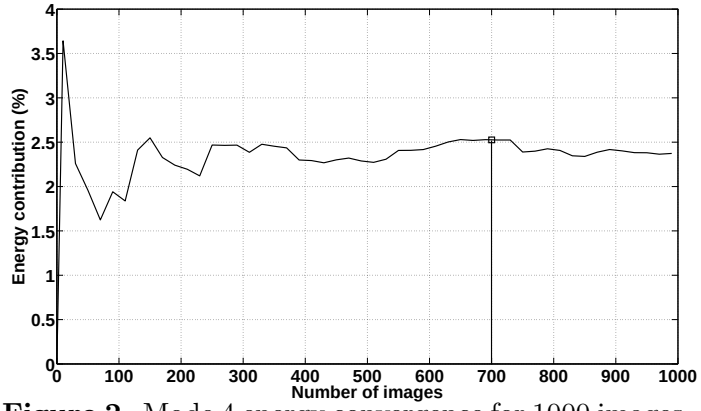

Figure 2. Mode 4 energy convergence for 1000 images, $\beta = 0.004$

The POD modes and their contributions for the reconstruction of the flow dynamics in terms of E_{mode} are shown in figure 3. It can be seen that the first mode is the most important one for both of the case studies. It can also be seen that the vapour zones are symmetrical for the pure cavitating flow, which is not the case for the aerated flow. The vertical lines show the closure region of the cavitation zone. For $\beta = 0$, the closure region is at $X^* = 3.1$, where for $\beta = 0.004$, the line is in the vicinity of $X^* = 3.7$. The zone beyond the cavity closure in figures 3(a') corresponds to the bubble-vapour mixture. The bubbles at the throat do not cut the cavitating zones. Rather, they break up due to the pressure gradient at the divergent zone and spread into extremely small bubbles, which interact mostly with the upper advected cavitating vapour. This is clearly visible in figure 3 (c') - the darkened zones beyond $X^* = 3.7$. On the contrary, the bottom cavitating zone stays intact, and thus the top and bottom vapour zones are not dynamically symmetrical. Based on the plots of the phase portraits of the temporal amplitudes, the observed phenomenon in figures (b) and (c) takes the form of an ellipse. The latter can be represented as two sine waves having the same frequency, 90° out of phase. In contrast, figures (b) and (d) display a phenomena having two frequencies with similar phases. In terms of energy contribution, one can see that modes (b),(c) are quite similar, which is also the case for (b'),(c'). It can be seen in figure 3 (b'), the cavitation zones are able to resume to their forms, once the detached air - vapour mixture is advected.

4. Conclusions and Perspectives

Side view images of aerated and non-aerated cloud cavity dynamics in a horizontal convergent divergent nozzle have been studied with a snapshot POD method. The modes account for more than 86% of the total energy for the aerated flow, and nearly 90% for the pure cavitation. Based on a robust mathematical instrument, the phase portraits are efficient for the cavitation regime exploration. The aeration inevitably influences the dynamics of the flow. The bottom vapour zone manages to maintain its correct dynamics, which is not the case for the other. The upper zone undergoes much more frequent cloud detachment than the one at the bottom. Lastly, the

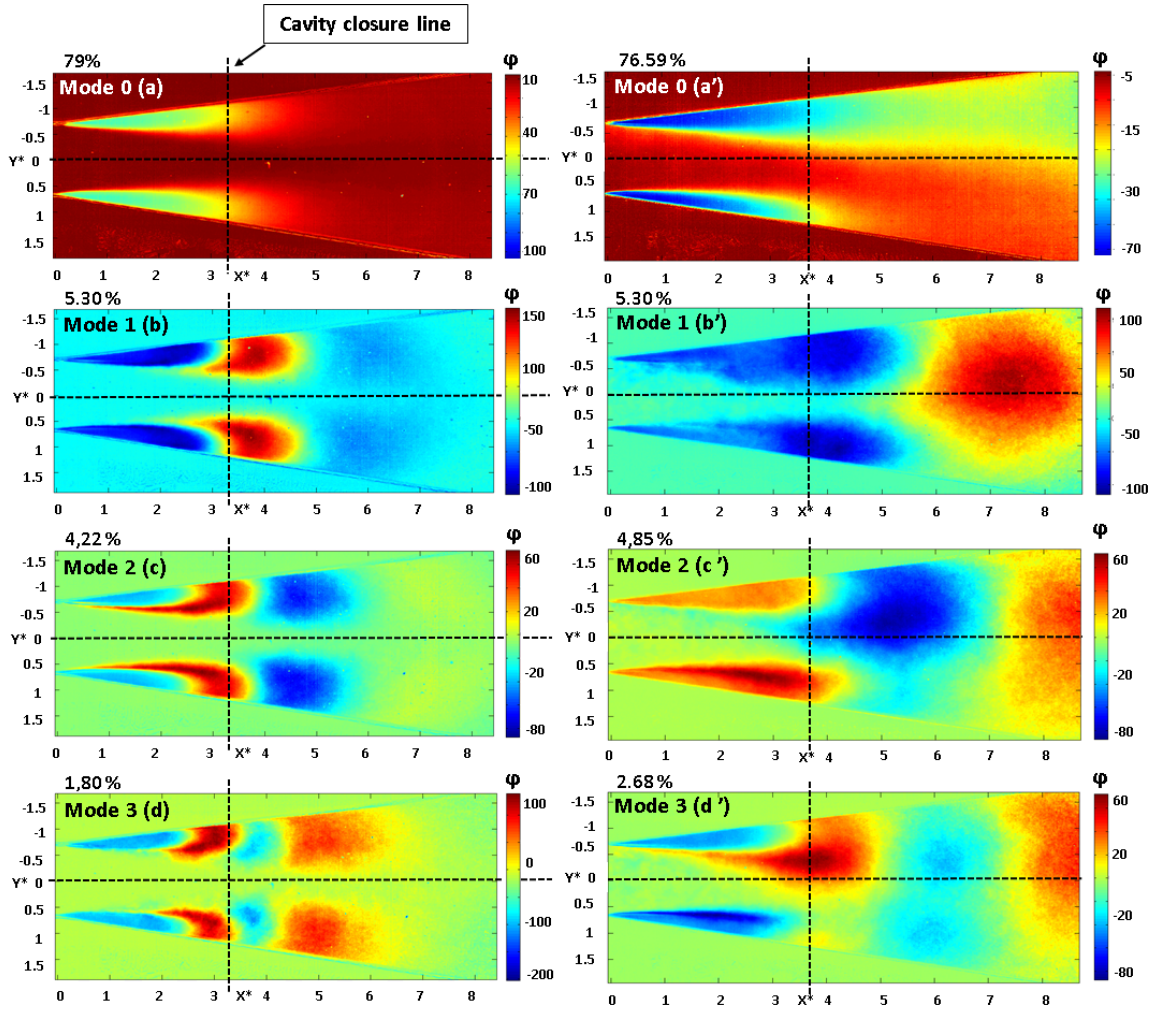

Figure 3. POD modes: $\beta = 0$ (left); $\beta = 0.004$ (right)

aggressiveness of the cloud cavitation, can be reduced by injecting controlled quantity of gas. In the foreseeable future, the authors plan to correlate pressure signals from the venturi throat section with the POD analysis from images.

Acknowledgments

The authors would like to acknowledge the financial support granted by SNECMA, part of SAFRAN group.

References

[1] Danlos, A., Méhal, J.E., Ravelet, F., Coutier-Delgosha, O., Bakir, F., Study of the cavitating instability on a grooved Venturi profile, *Journal of Fluids Engineering*, 2014, **136**(10), pp.1—10.

[2] Dunn, P.F., Thomas, F.O., Davis, M. P., Dorofeeva, I.E., Experimental characterization of aviation-fuel cavitation, *Physics of Fluids*, **22**(2010), 117102.

[3] Berkooz, G., Holmes, P., Lumley, J., The proper orthogonal decomposition in the analysis of turbulent flows, *Annual Review of Fluid Mechanics*, **25**(1993), pp.539—575.

[4] Danlos, A., Ravelet, F., Coutier-Delgosha, O., Bakir, F., Cavitation regime detection through Proper Orthogonal Decomposition: Dynamics analysis of the sheet cavity on a grooved convergent-divergent nozzle, *International Journal of Heat and Fluid Flow*, **47**(2014), pp.9—20.

[5] Dular, M., Bachert, B., Stoffel, B., Sirok, B., Relationship between cavitation structures and cavitation damage, *Wear*, **257**(2004), pp.1176—1184.